Cellulose (2019) 26:3167–3181
https://doi.org/10.1007/s10570-019-02292-5

ORIGINAL RESEARCH

Surface modification of cellulose nanocrystal using succinic anhydride and its effects on poly(butylene succinate) based composites

Canqing Wu · Xuzhen Zhang · Xiuhua Wang · Qingwen Gao · Xinan Li

Received: 6 July 2018 / Accepted: 25 January 2019 / Published online: 1 February 2019

Abstract Cellulose nanocrystals (CNCs) extracted from microcrystalline cellulose, were modified by succinic anhydride to give succinic CNCs (SCNCs). Successful surface modification of SCNCs was confirmed by results of FTIR, FE-SEM, contact angle measurement and dispersity test, and SCNCs were then subjected to melt blending with poly(butylene succinate) (PBS) to prepare nanocomposites. Meanwhile, PBS/CNC nanocomposites were also prepared through same procedure as references. The morphology, thermal and mechanical properties and crystallization properties of PBS/SCNC nanocomposites with increasing SCNCs content from 0 to 7 wt% were investigated. PBS/SCNC nanocomposites exhibit better thermal stability than that of PBS/CNCs, which is mainly ascribed to less sulfate groups on CNC surfaces and more hydrogen bond effects between PBS carbonyl groups and ester groups from SCNCs. Young's modulus and yield strength of PBS/SCNCs are higher than that of PBS/CNC nanocomposites, which is primarily attributed to the homogeneous dispersion of SCNCs in PBS matrix, confirmed by FE-SEM images. This work is valuable for design of PBS-based nanocomposites with enhanced thermal and mechanical properties.

Canqing Wu and Xuzhen Zhang have contributed equally.

C. Wu · X. Zhang (✉) · X. Wang · Q. Gao · X. Li
The Key Laboratory of Advanced Textile Materials and Manufacturing Technology of Ministry of Education, College of Materials and Textile, Zhejiang Sci-Tech University, Hangzhou 310018, China
e-mail: donghuaihe@163.com

Graphical abstract

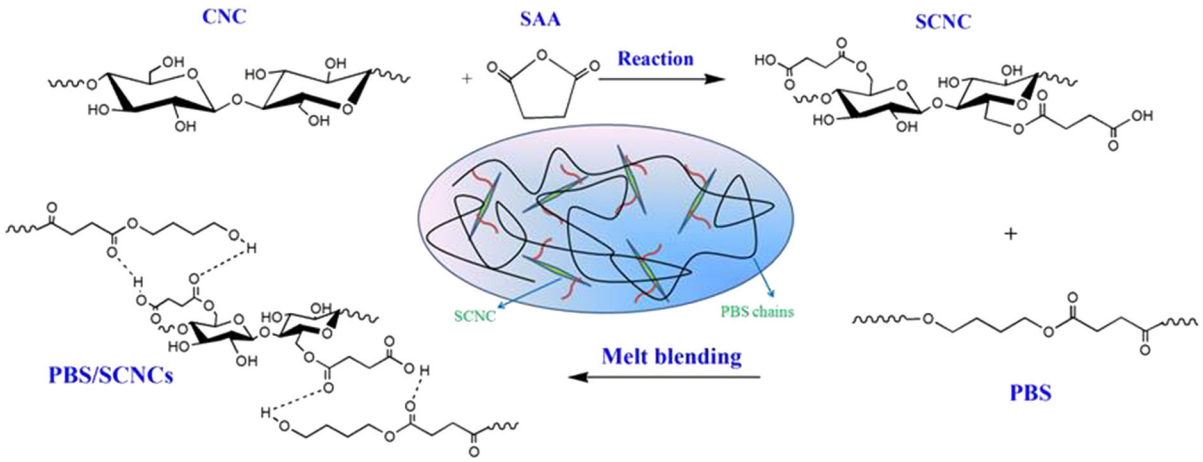

Keywords Cellulose nanocrystals · Poly(butylene succinate) · Succinic anhydride · Modification · Nanocomposites

Introduction

In recent years, owing to increasing depletion of petroleum resources and the environmental pollution caused by non-biodegradable plastics, the research of sustainable polymeric materials has attracted a great deal of attention (Ragauskas et al. 2006). Nowadays, various biodegradable polymers, such as poly(lactic acid) (PLA), poly(vinyl alcohol) (PVA) and poly(3-hydrobytyrate-*co*-3-hydroxyvalerate) (PHBV), have been reviewed extensively in several publications (Avolio et al. 2015; Nampoothiri et al. 2010; Paralikar et al. 2008). Among these biodegradable polyesters, PBS has better processability and flexibility compared to other candidates. However, the modulus and tensile strength of PBS are low, which highly restricts its further application (Liang et al. 2010).

In order to improve the mechanical properties of PBS, numerous reports have been published focusing on biomass fillers as reinforcing agents in PBS materials, such as corn starch (Flores et al. 2009), spun silkworm silk fabric (Chen et al. 2017), corn silk (Likittheerakarn et al. 2017) and ramie fiber (Zhou et al. 2014). Compared to other biomass fillers, cellulose nanocrystals (CNCs), extracted from purified cellulose fiber after a complete dissolution of the non-crystalline fractions by chemical hydrolysis (Ng et al. 2015), have high mechanical strength, surface area and higher modulus(138–150 GPa), which is close to theoretical modulus of perfect crystal (Silverio et al. 2013). Therefore, CNCs can be used to reinforce PBS and retain the biodegradable properties of PBS.

As all known, the polarity of CNCs is strong due to great amount of hydroxyl agents on the surface. When CNCs are added into non-polar matrices, the strong polarity of CNCs results in a series of problems: low interfacial compatibility with the matrices, low moisture resistance/barrier, and self-aggregation by hydrogen bonding (Hashaikeh et al. 2015). To solve these problems, surface modification of CNCs is a common and simple method to reduce the surface polarity of CNCs and obtain good dispersion in polymeric matrices (Angellier et al. 2005). A range of available methods have been proposed for modification of CNCs, including oxidations (Coseri et al. 2013), esterification (Braun et al. 2012), amidations (Fujisawa et al. 2011), ethericatons (Motte et al. 2011) and carbamations (Shang et al. 2013). For instance, Fortunati et al. (2012) have employed surfactants on CNC surfaces to facilitate dispersion of CNCs in PLA matrix. Similarly, Poaty et al. (2014) have reported a preparation of surface modifications on CNCs using alkyl quaternary amines or acryloyl chloride in simple conditions, the results showed that those chemical modifications do not change the CNCs main structure, and the modified CNCs were better dispersed in aqueous coating. In other approach, CNCs were

grafted by lactic acid oligomers to improve the dispersion in the PLA matrix (Glova et al. 2016). However, as we known, there is few researches focused on the reinforcement of CNCs in PBS matrix. Hu et al. (2015) have carried out surface modification on the CNCs via the esterification to promote the compatibility between modified CNCs and PBS matrix. The results show that with the introduction of 5 wt% modified CNCs, the specific flexural strength and modulus of nanocomposites increased by 75.7% and 57.2% comparing with the neat PBS materials. However, the improvement of mechanical properties is limited, mainly due to the lack of strong chemical interaction between matrix and fillers. Recently, in order to improve the dispersion and compatibility between PBS and poly(lactic acid) (PLA) composites, Zhang and Yong (2016) prepared PBS-grafted cellulose nanocrystals (PBS-*g*-CNCs) via in situ polymerization, and observed that the addition PBS-*g*-CNCs could improve the dispersion and interfacial compatibility in both PBS and PLA phases, and both storage modulus and glass translation temperature of PBS/PLA composites are increased by PBS-*g*-CNCs. However, it is too complicated and time-consuming to improve the compatibility of polymer matrix through in situ polymerization.

In the present paper, CNCs were prepared through sulfuric acid hydrolysis of microcrystalline cellulose (MCC). Succinic anhydride (SAA), sharing similar chemical structure with succinic acid repeated unit in PBS main chain, is grafted onto CNC surfaces to reduce polarity of CNCs. The chemical structure, surface polarity, thermal properties and crystallization properties of CNCs after modification are tested using fourier transforms infrared spectroscopy (FTIR), field-emission scanning electron microscopy (FE-SEM), thermal gravimetric analysis (TGA), contact angle, and wide angle X-ray diffraction analysis (WAXD) methods. Subsequently, both modified CNCs and pristine CNCs are added into PBS via melt blending, respectively. The effects of degree of surface substitution (DS) for CNCs and CNC content on morphology, mechanical properties, thermal properties and crystallization properties of PBS/CNCs nanocomposites are investigated.

Experiment

Materials

Poly(butylene succinate) PBS with a density of 1.26 g/cm^3 and melt flow index (MFI) 18.3 g 10 min^{-1} (190 °C, 2.16 kg) was produced by Shaoxing Global Chemical Fiber Co., Ltd.(China). Microcrystalline cellulose (MCC) was purchased from Sinopharm Chemical Reagent Co., Ltd. (China). Pyridine was purchased from Tianjin Kemiou Chemical Reagent Co., Ltd. (China). Acetone (99%) and sulfuric acid (98%) were purchased from Zhejiang Sanying Chemical Reagent Co., Ltd. (China). Ammonia (25%), succinic anhydride (SAA, 99%) and 4-dimethylaminopyridine (DMAP 99%) were purchased from Aladdin Industrial Inc. (China). Pyridine was purified by anhydrous calcium chloride. All other solvents and reagents were used without further purification.

Extraction of cellulose nanocrystals (CNCs)

CNCs were prepared by sulfuric acid (H_2SO_4) hydrolysis of MCC with similar procedure reported in other research (Hamad and Hu 2010). In brief, the MCC was dispersed in 64 wt% of sulfuric acid at the ratio of 8.75 ml of the sulfuric acid solution/g MCC (Xue et al. 1998). After that, the suspension was stirred constantly at 48 °C for 6 h under nitrogen atmosphere in a flask. At the end of the reaction, the suspension was diluted by an amount of distilled water to stop the hydrolysis. After the hydrolysis, the resulting suspension was purified by successive centrifugation with distilled water. The pH of the suspension was adjusted by adding ammonia dropwise to pH 7, and finally CNCs were obtained after the freeze-drying treatment.

Surface esterification modification of CNCs

The esterification was carried out in pyridine medium under nitrogen atmosphere. Freeze-dried CNCs were dispersed in pyridine at a concentration of 1 g/20 ml (Lin and Dufresne 2014; Miao and Hamad 2016), followed by ultrasonic treatment for 15 min. SAA and the catalyst, DMAP, were then added into the suspension sequentially, and DMAP was added at 1 wt% of CNCs. The mass ratios of CNCs to SAA were 1:0.5, 1:1, 1:1.5, 1:2, respectively. The esterification lasted at 80 °C for 4 h. After the reaction, the

suspension was washed by acetone and water several times to remove unreacted succinic anhydride and SCNCs were obtained after freeze-drying suspension. The SCNC samples were denoted as SCNC-0.5, SCNC-1, SCNC-1.5 and SCNC-2, respectively.

Preparation of nanocomposites materials

Prior to melt blending, SCNC-2, theoretically having better hydrophobicity than other samples, were vacuum-dried for 12 h at 60 °C along with PBS and CNCs. After that, given amounts of CNCs and SCNC-2 were melt blended with PBS using a RM-200 C mixer rheometer (Harbin Hapro Electric Technology Co., Ltd, China) at the rotation rate of 60 rpm and 120 °C for 10 min. The nanocomposites were compressed molded as sheet at 20 MPa at 140 °C for 5 min pressure using hot-press machine (Zhejiang ShuangLi Group Co., Ltd, China). After that, all nanocomposites sheets were cut into bone-shaped specimens. PBS/CNC and PBS/SCNC-2 nanocomposites were prepared with the presence of various CNC and SCNC-2 content from 0 to 7 wt(%) and named as PBS/CNC(99/1), PBS/CNC(97/3), PBS/CNC(95/5), PBS/CNC(93/7), PBS/SCNC(99/1), PBS/SCNC(97/3), PBS/SCNC(95/5), PBS/SCNC(93/7), respectively. All nanocomposites sheets were cut into standard bone-shaped specimens for mechanical tests after being cooled down (Fig. 1).

Characterization

Morphology of CNCs, modified CNCs and nanocomposites were characterized by field emission scanning electron microscopy (FE-SEM) (Carl Zeiss SMT Pte Ltd), Digital image analysis (ImageJ Software) was used in order to measure the dimensions of the samples. Before testing, all samples of PBS-based composites were freeze fractured by immersing into liquid nitrogen and then sputter coated with a layer of gold.

Fourier transforms infrared spectroscopy (FTIR) spectrograms of the powdered CNCs and SCNCs, as well as all the PBS based nanocomposites sheets, were obtained on an FTIR 5700 spectrometer (Thermo Electron Corp., USA). The powdered CNCs and SCNCs were measured using a KBr pellet method in the range of 500–4000 cm^{-1} with OMNIC software, and PBS based composites sheets were scanned in the range of 500–4000 cm^{-1} using OMNT reflections accessories. The background was subtracted from the spectra automatically each time.

Solid state ^{13}C cross polarization magic spinning (CP-MAS) NMR experiment were performed on a Avance400 solid instrument spectrometer with a MAS rate of 6 kHz, at a frequency of 75.5 MHz for ^{13}C NMR. All spectrum were run for 2 h (3000 scans).

Degree of substitution (DS) values of modified CNCs were determined by titration method (Content 1997; Ogawa et al. 1999). Dry modified CNC samples (0.1 g) were transferred to a 100 ml conical flask containing 15 ml distilled water, followed by ultrasonic treatment for 15 min. Phenolphthalein was added into suspension as an indicator, and then NaOH (0.1 mol/l) solution was added to retain the reddish color under the ice water bath. Subsequently, 30 ml NaOH (0.5 mol/l) was added. The solution was maintained at a temperature of 40 °C for 2 h, and then titrated with HCl (0.5 mol/l) solution until the red color faded. The volume of HCl (V_1) was recorded. Original CNC powder was also tested as blank experiment, then the volume of HCl (V_2) was recorded. The degree of substitution (DS) was calculated from the following equation:

$$DS = \frac{81 \times (V_2 - V_1)}{100}$$

Surface hydrophilicity of CNCs and modified CNCs were evaluated at room temperature by measuring the contact angle of a small water drop (ca. 5 µl) using the DSA20 contact angle measurement (Kruss Corp, Germany). The powdered CNCs and modified CNCs were compacted under a pressure of 10 MPa with a KBr press to obtain samples with smooth surfaces.

Images of the sessile drops were processed using drop shape analysis software. CNCs and modified CNCs were added into mixed solvent of chloroform/water (50/50). After ultrasonic treatment for 15 min, the dispersity of suspension was evaluated by visual observation. Zeta Potential measurement for samples at pH = 7 values were measured using Malvern Zetasizer 2000 (Malvern Instruments Ltd., UK). The CNCs and SCNC-2 were re-dispersed in deionized water; their concentrations were adjusted to 0.001 g/g (0.1 wt%), and then sonicated using an ultrasonic processor (300 W, 100 s). Every zeta potential was averaged over 10 measurements.

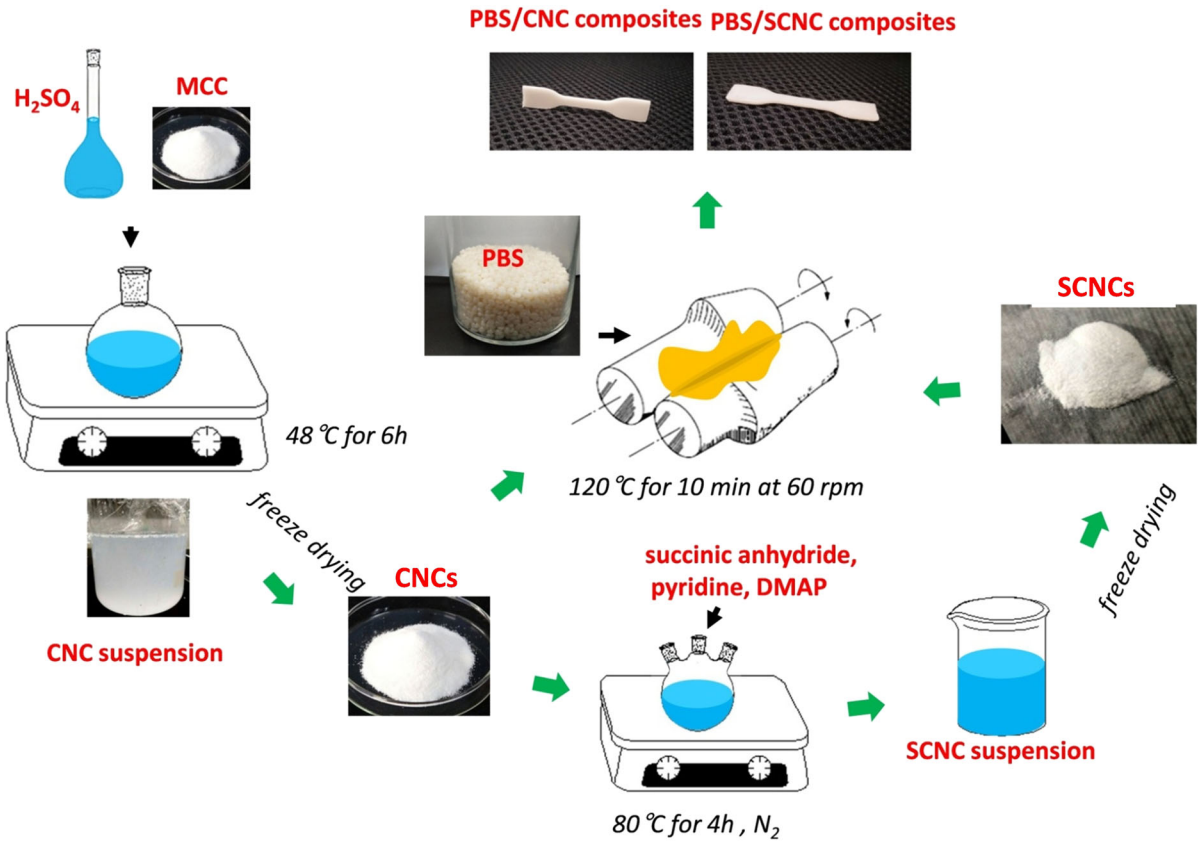

Fig. 1 Schematic of PBS-based composites production routes

Elemental analysis was performed at elemental analyzer (Flash EA112, Italy). The carbon (C%), hydrogen (H%) and sulfur (S%) contents for both CNC and SCNC-2 samples were measured.

Crystallization behavior of neat PBS and composites was investigated by differential scanning calorimeter (DSC) instrument (Mettler Toledo Instrument Co., Ltd, Switzerland). Each sample was firstly heated from 20 to 150 °C at a rate of 20 °C/min and maintained at 150 °C for 3 min to erase previous thermal history. In order to avoid crystallization of composites sample, the sample was cooled to − 50 °C at a cooling rate of 50 °C/min and maintained 3 min. Subsequently, the crystallized sample was heated to 150 °C and cooled again to 20 °C at a rate of 20 °C/min to evaluate the glass transition temperature, melt point and crystallization behavior of the nanocomposites, respectively. The crystallinity (X_c) was calculated from the following equation during the second heating scan:

$$X_c(\%) = \frac{\Delta H_m}{(1-\mu)\Delta H_m^0} \times 100$$

where ΔH_m is the enthalpy for melting of PBS-based nanocomposites, which was determined from the second heating scan. ΔH_m^0 = 200 J/g, the heat of fusion 100% crystalline PBS (Luzi et al. 2016; Miyata and Masuko 1998; Papageorgiou and Bikiaris 2005) and (1 − μ) is the weight fraction of PBS in the sample. Thermal stability of CNC and nanocomposites was tested on thermogravimetric analysis (TGA) (Mettler Toledo Instrument Co., Ltd, Switzerland). All samples were heated from 25 to 700 °C at a heating rate of 20 °C/min under nitrogen atmosphere.

Neat PBS, PBS/CNC and PBS/SCNC nanocomposites were cut into dumbbell-shaped specimen with width of 4 mm and thickness of 1 mm, and had been stored at room temperature for 24 h before measurement. Mechanical tests were performed on a tensile device (Instron 3367, Instron Corp., USA) at 19 °C and 45% humidity. According to ASTM D 882-10,

dumbbell-shape samples were tested at a crosshead speed of 20 mm/min. Five specimens were test for each samples to get average values.

Results and discussion

Morphology of CNCs (SCNC-2)

Morphology of SCNC-2 was observed by FE-SEM and the image was compared with that of pristine CNCs in Fig. 2. The length and diameter of these nanocrystals were determined by using digital image analysis (ImageJ). Both the obtained histograms and cumulative curves are shown in Fig. 2a2, a3, b2, b3. Mean size of CNCs is evaluated as 283.4 nm in length and 21.7 nm in diameter. After modification, length of CNCs is 287.2 nm and diameter is 25.1 nm, respectively. It can be seen that there is no obvious change in the dimension of individual CNCs before and after modification. Rod-like shape of CNCs is preserved after modification. Similar dimensions have reported in previous literature (Espino-Pérez et al. 2013).

Chemical structure of CNCs (SCNCs)

Zeta potential and elemental analysis were performed. Table 1 shows zeta potential and elemental content of CNC and SCNC-2 samples. Zeta potential of original CNCs prepared by acid hydrolysis are − 30.2 mV while that of SCNC-2 are − 8.4 mV. Weight percentage of sulfur (S) decreased from 0.20% in CNCs to 0.06% in SCNC-2. The sulfur element assigned to the sulfate groups on the surface of CNCs was removed after modification, which indicated the possible solvolytic desulfation during this treatment (Jiang et al. 2010).

Table 1 Characteristics of the original CNCs and SCNC-2 samples

Sample	Zeta potential (mV)	Elemental analysis		
		C%	H%	S%
CNCs	− 30.2	41.10	5.95	0.20
SCNC-2	− 8.4	41.37	6.23	0.06

FTIR spectra of both CNCs and SCNC-2 are shown in Fig. 3b. Typically, the spectra exhibit peaks contributed by functional groups of CNCs. Broad peak at 3330 cm^{-1} is attributed to the presence of hydroxyl groups (–OH). The peaks mentioned above keep decreasing with increasing SAA content. Considering both CNCs and SCNC-2 have been dried at most, the decrease of the peaks at 3330 cm^{-1} should be ascribed to the partial disappearance of (–OH) groups after modification. Besides that, consistent with the occurrence of modification by esterification, all SCNCs

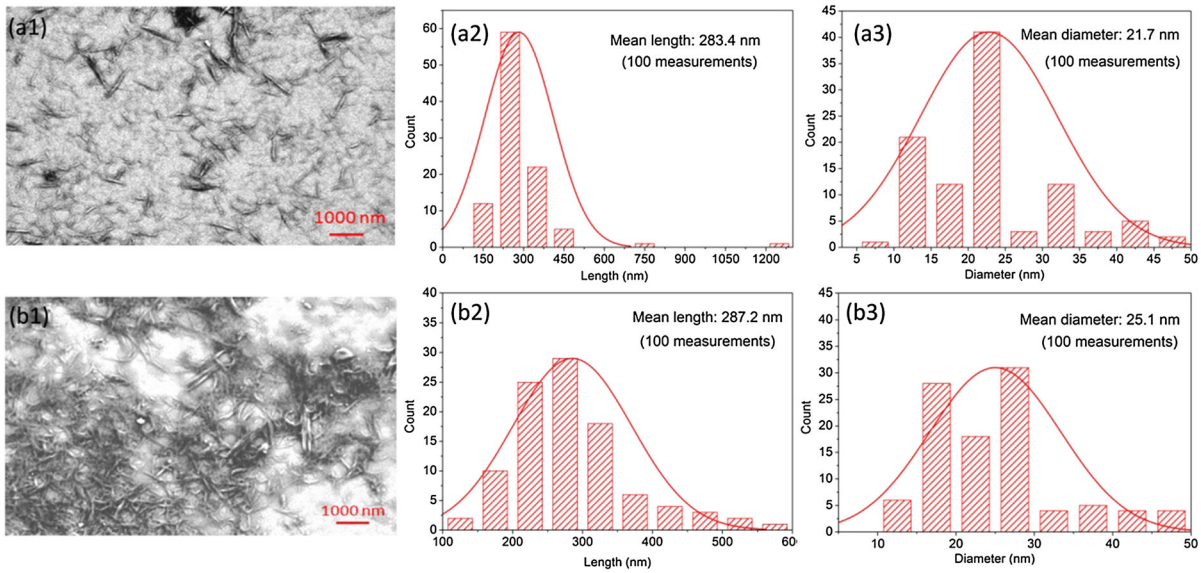

Fig. 2 FE-SEM images of **a1** CNCs, **b1** SCNC-2, **a2** length, **a3** diameter distribution of CNC and **b2** length, **b3** diameter distribution of SCNC-2

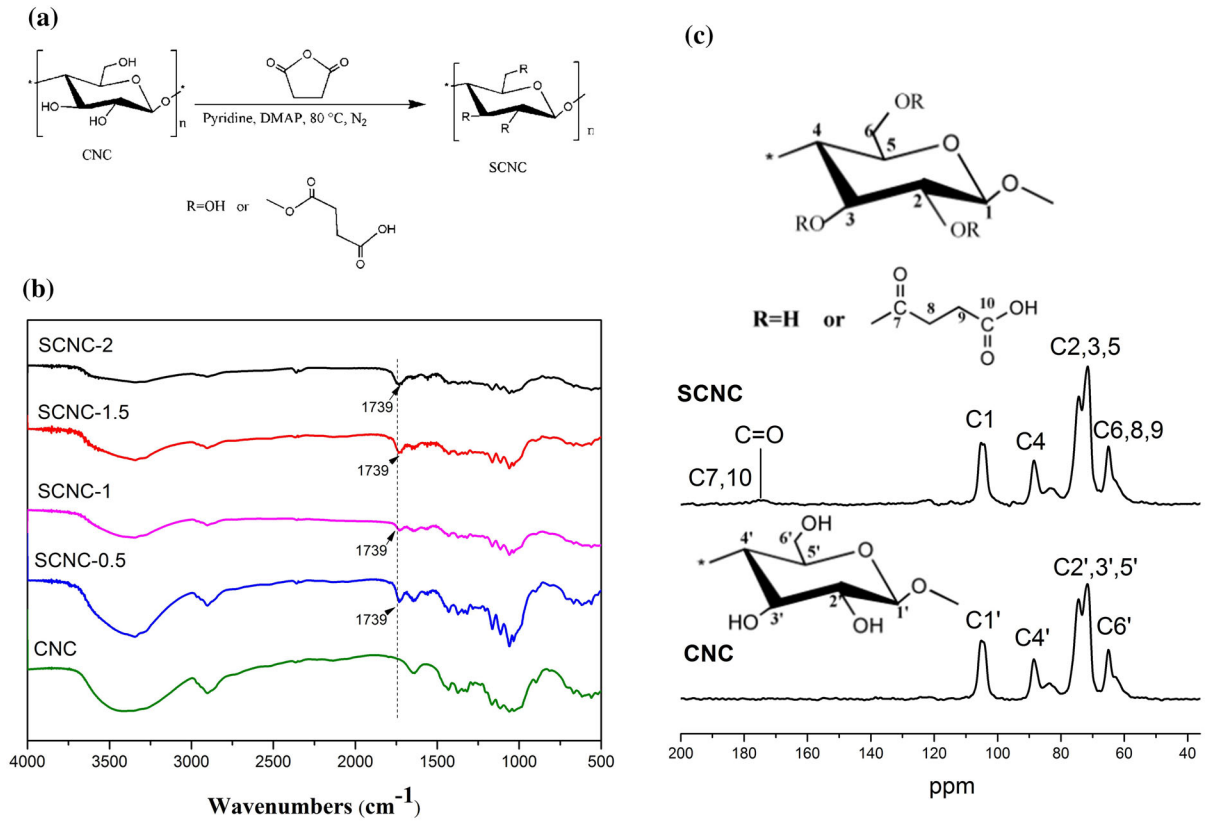

Fig. 3 Scheme of grafting reaction of SAA on CNC surface (**a**). FTIR spectra of CNCs before and after modified by increasing amount of SAA (**b**). ^{13}C CP-MAS NMR spectra of original CNCs and SCNCs (**c**)

series show new peaks at 1739 cm^{-1} that correspond to the (–C=O) ester band. Above this, CNCs is successfully modified by SAA.

Modified CNCs were further characterized by ^{13}C CP-MAS NMR spectroscopy (as shown Fig. 3c). As in a previous report (Lin et al. 2011), chemical shifts of carbon atoms from original CNCs were C1′ (105 ppm), C4′ crystalline (88 ppm), C4′ amorphous (83 ppm), C2′,3′,5′ (72-74 ppm), and C6′ (65 ppm). After esterification, a new chemical shift located at 175 ppm, which assigning to C7,10 (–C=O) of the carbonyl groups on SCNC, confirming successful modification of CNCs.

Surface polarity of CNCs and SCNCs

DS of CNCs modified with increasing amount of SAA is shown in Fig. 4a. SCNCs show a steep increase from 0 to 0.68% in DS with increasing SAA amount. When ultrasonic oscillated in a mixed solvent of water/chloroform, CNCs and SCNCs show different dispersion as shown in inserted image in Fig. 4a. CNCs disperse in waster phase while SCNCs disperse in chloroform phase, which has poorer polarity than water. This phenomenon illustrates that surface polarity of CNCs has been weakened after esterification, which is corresponding to results of FTIR. Figure 4b shows the values of water contact angle measured for CNCs and SCNCs for a second, contact angle value of the original CNCs is about 48°, but that of SCNCs keeps increasing with increasing DS. The results show that surface modification can significantly improve the hydrophobicity of CNCs. One of the main reason is that high DS leads to less hydroxyl groups on CNC surfaces (Bendahou et al. 2014).

Chemical structure of PBS based composites

ATR FTIR spectrum were recorded for PBS and the PBS-based composites film in order to investigate

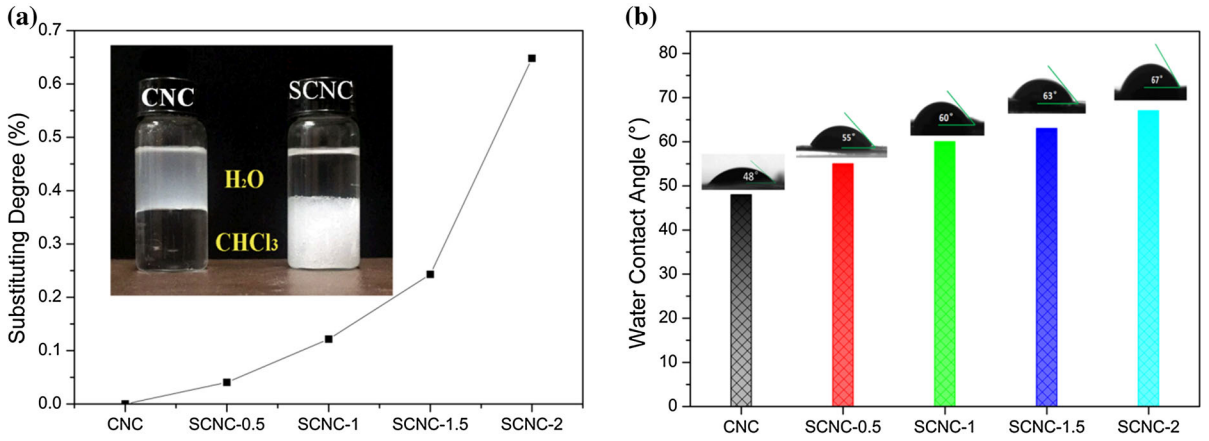

Fig. 4 **a** DS of CNCs after modification with increasing amount of SAA. The inserted image shows distribution of CNCs and SCNCs in water/chloroform mix solvent (the upper solvent is deionized water and the lower solvent is chloroform). **b** Water contact angle of CNCs before and after modified with different amount of SAA

hydrogen bonds between the CNCs (SCNCs) and PBS. FTIR spectrum are shown in Fig. 5a. For PBS-based nanocomposites, carbonyl-stretching region within 1650–1800 cm^{-1} in the infrared spectra is very sensitive to the hydrogen-bond formation. Peaks at 1712 cm^{-1} are assigned to characteristic carbonyl groups from all PBS composites, while CNCs and SCNCs show weak absorption in this region as shown in Fig. 3b. Therefore, changes can be observed in this region when the carbonyl groups environment of polyesters changes, such as the formation of hydrogen bonds (Zhu et al. 2003). When CNCs or SCNCs loading increased to 1 wt%, a new peak appears at 1689 cm^{-1}, indicating possible hydrogen bonding between carbonyl groups (–C=O) of PBS and hydroxyl groups (–OH) of CNCs or SCNCs. And the hydrogen bonding schematic representation was presented in Fig. 5b. Similarly, hydrogen bonding was also detected between PBS and ramie fiber (Zhou et al. 2014).

Morphology of PBS based composites

Figure 6 shows FE-SEM images for the cryo-fractured surface of PBS based nanocomposites with different CNCs and SCNCs loadings. Neat PBS showed a

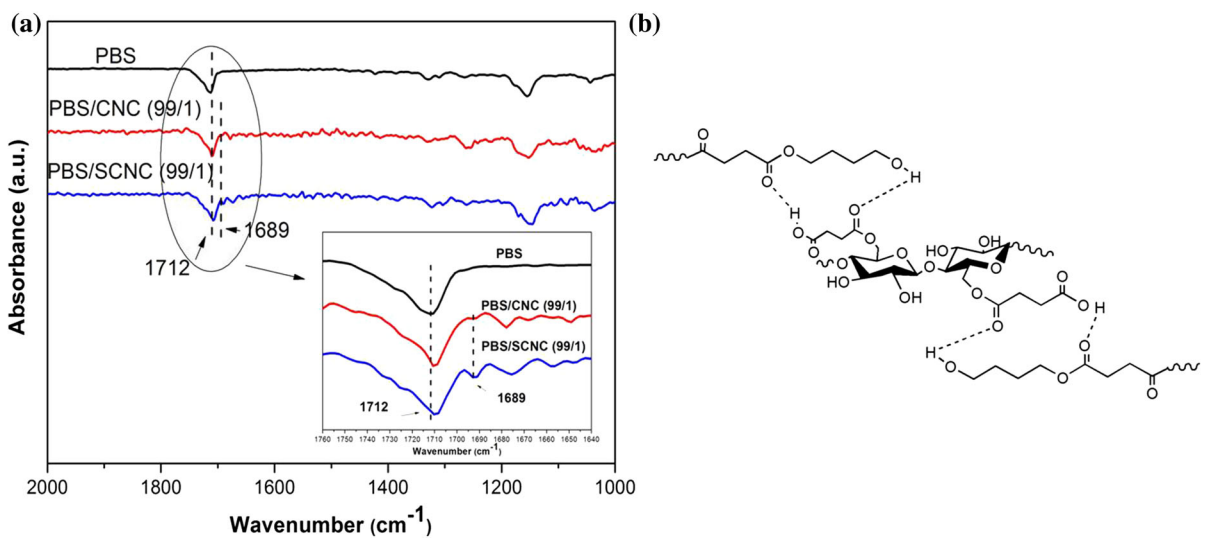

Fig. 5 FTIR spectra of PBS and PBS-based nanocomposites (**a**). Schematic representation of interaction between SCNCs and PBS (**b**)

smooth morphology as shown in Fig. 6a. When CNCs (SCNCs) were introduced at a loading lower than 3 wt%, the nanofillers can disperse homogeneously in PBS matrix as shown in Fig. 6b, c, e, f. Thereafter, PBS/CNC nanocomposites show coarse surface and more self-aggregation when continue increasing CNC loadings as shown in Fig. 6d. Especially, blending 5 wt% of CNCs into the neat PBS resulted in large agglomerates of CNC particles. Nevertheless, no self-aggregation is observed on surface even with SCNCs loading increased to 5 wt% as shown in Fig. 6g. The results show that SAA modification partly improved the dispersion of CNC in PBS matrix, which agreed well with dispersibility in a mixed solvent of water/chloroform. Similar morphology phenomenon can be also observed for PLA/CNC (Zhou et al. 2018a).

Thermal properties of PBS-based nanocomposites

DSC measurements were carried out to investigate the effect of CNCs on the crystallization and thermal properties of nanocomposites. As shown in Fig. 7a, b, crystallinity (X_c) of PBS-based nanocomposites is slightly increased compared with neat PBS, indicating that incorporation of CNCs (SCNCs) could act as nucleator to enhance crystallinity of PBS even with very small addition. However, the crystallinity of PBS/SCNC composites is slightly lower than that of PBS/CNC. Actually, compatible fillers are not propitious to nucleation in polymer matrix while gaining dispersion. This result is attributed to the fact that the number of interface/contact filler with the matrix is much more important once modified CNCs are used contrary to CNCs and its aggregates. Similar results have also been reported by other researchers (Espino-Pérez et al. 2013; Vahik and Pochan 2004).

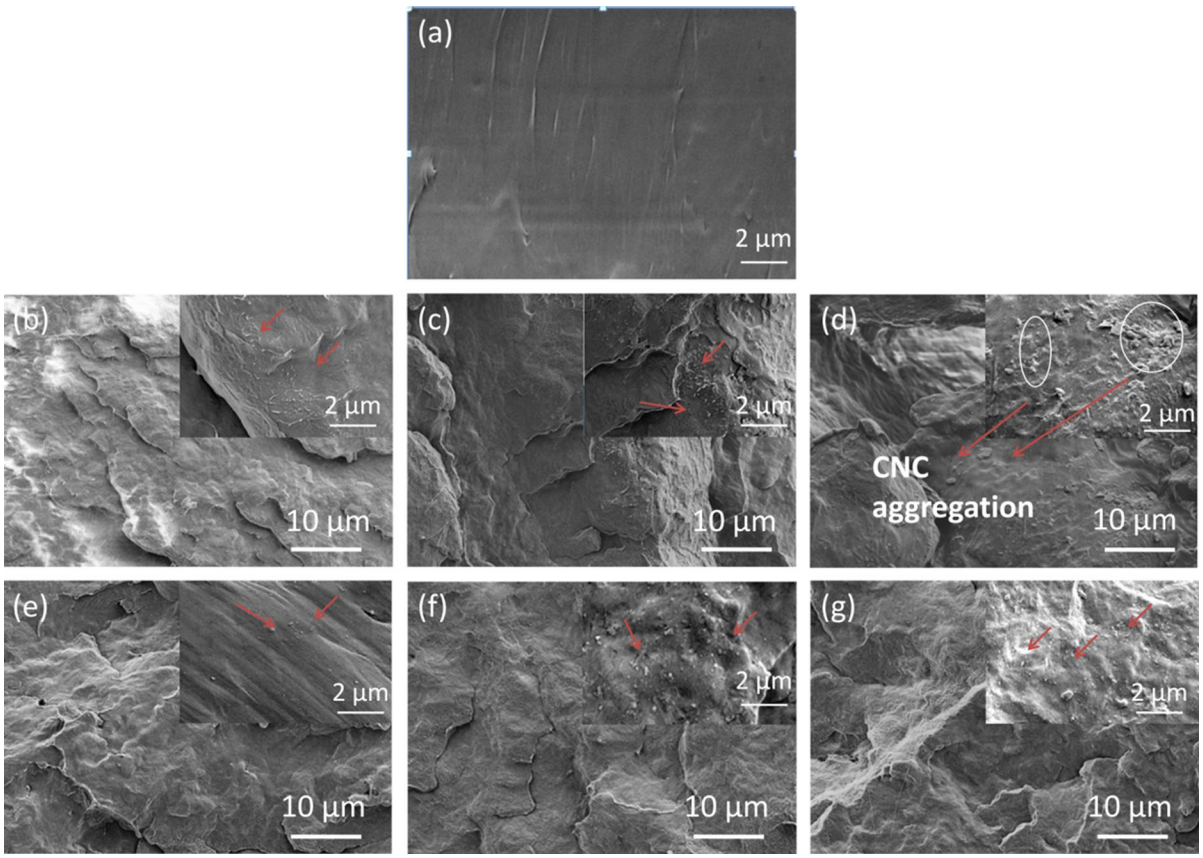

Fig. 6 FE-SEM images for cryo-fractured surface of neat PBS (**a**), PBS/CNC(99/1) (**b**), PBS/CNC(99/3) (**c**), PBS/CNC(95/5) (**d**), PBS/SCNC(99/1) (**e**), PBS/SCNC(97/3) (**f**), and PBS/SCNC(95/5) (**g**) [inserted images are observed under high resolution and dark arrows are used to point out CNCs (SCNCs) or their aggregations]

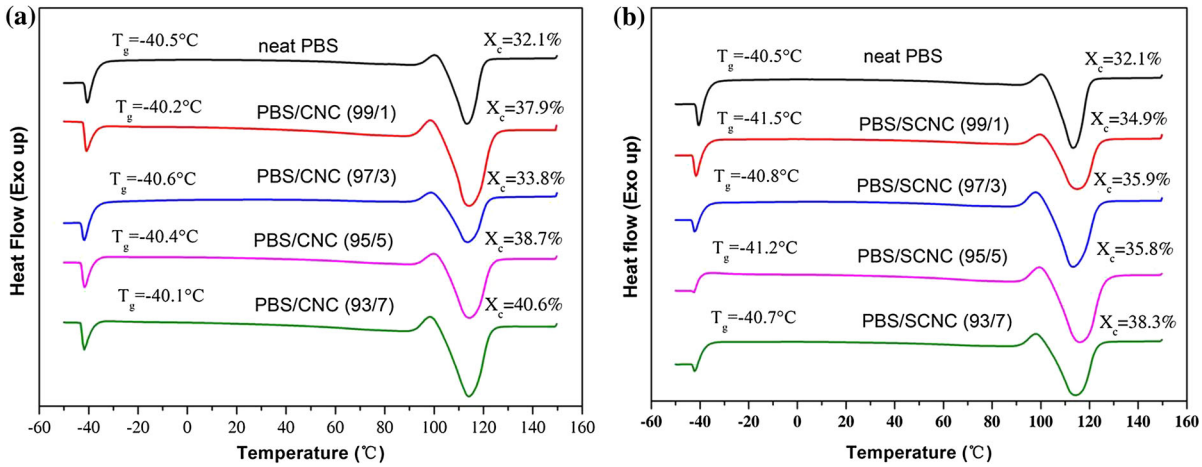

Fig. 7 DSC the second heating curves of neat PBS and its nanocomposites

The thermal stability of nanofillers greatly affects processability and properties of PBS-based composites. Thus, the effect of CNCs (SCNCs) on the thermal stability of PBS-based nanocomposites was studied by TGA under nitrogen atmosphere. The TGA and derivative DTG curves are shown in Fig. 8a–d, and corresponding data are summarized in Table 2. $T_{d(99\%)}$, $T_{d(97\%)}$ and $T_{d(95\%)}$ are temperature with 99%, 97% and 95% sample mass retention, respectively. T_{max} stands for the temperature at fastest thermal degradation rate. In Fig. 8a, b, a main weight loss stage is attributed by CNCs molecular decomposition, and this stage moves to higher temperature during SCNCs decomposition. In addition, a new weak stage appears in SCNCs decomposition curve, which might be ascribed to the decomposition of SAA molecules on CNC surfaces. Similar results have been reported previously (Nagalakshmaiah et al. 2016; Zhou et al. 2018b). Residual mass of CNCs at 700 °C is higher than that of SCNCs, which is caused sulfuric acid residue in CNCs. Sulfuric acid is a well-known dehydration catalyst and facilitated the char residue (Flores et al. 2009; Likittheerakarn et al. 2017; Tang et al. 2014). Zeta potential value of original CNCs prepared by acid hydrolysis is − 30.2 mV while that of SCNCs is − 8.4 mV, and the weight percentage of sulfur (S) decreased from 0.20% in origin CNCs to 0.06% in SCNC-2 (as shown in Table 1). Zeta potential measurements and elemental analysis confirmed the reduction of sulfate groups on the CNC surfaces after modification, and the thermal decomposition of CNCs considerably shifts to higher temperature when this sulfate groups are reduced. Since the functionalization leads to the reduction of many sulfate groups on the CNC surfaces (Pinheiro et al. 2017), the improved thermal stability of SCNCs seems to have this origin.

Thermal decomposition $T_{d(99\%)}$, $T_{d(97\%)}$ and $T_{d(95\%)}$ of PBS/CNC composites have an decreasing tendency with addition of CNC contents. Only when PBS/CNC (99/1), it seems that thermal stability of PBS/CNCs is higher than that of neat PBS as shown in Fig. 8c. The decrease of thermal decomposition temperature of PBS/CNC composites might be mainly attributed to the fact that sulfate groups on the surface of CNCs during the acid hydrolysis compared with SCNCs can accelerate the thermal degradation of PBS. Similar thermal decomposition behavior was also observed for the PLA/CNC composites (Spinella et al. 2015). Conversely, the thermal decomposition temperature is clearly shifted to higher temperature for PBS/SCNC composites compared to that of PBS/CNC composites as shown in Fig. 8c, d. This results show that char and gases evolved from SCNCs degradation may delay thermal decomposed of PBS matrix, Similar phenomenon have been also demonstrated (Jiménez and Ruseckaite 2007). Meanwhile, more hydrogen bond effects maybe present between the polymer carbonyl groups and ester groups from SCNCs. Similar results have been demonstrated for PLA-based nanocomposites (Fortunati et al. 2010). In addition, the homogeneous dispersion of SCNCs in PBS matrix could prompt the more effective barrier effect than that of CNCs, which restricts polymer chains mobility and

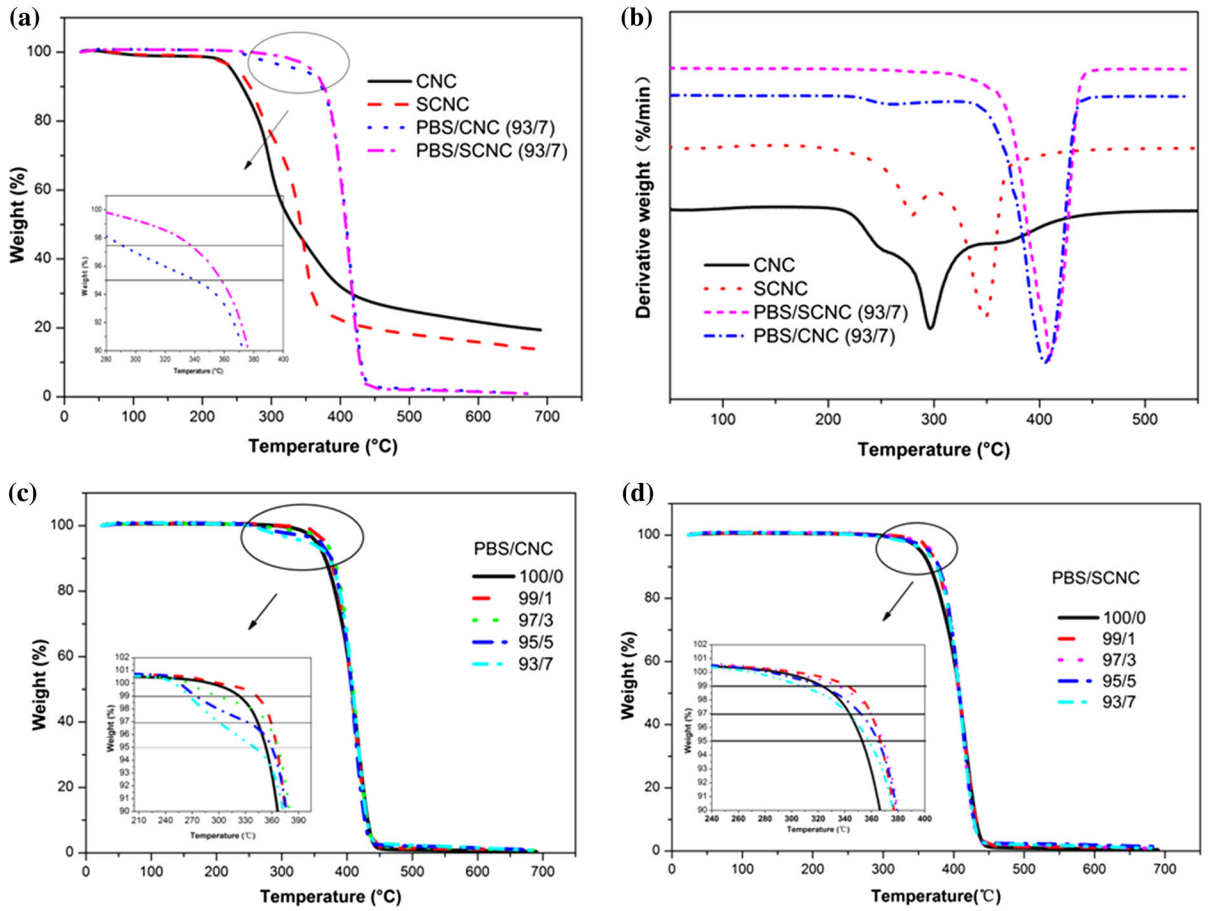

Fig. 8 TGA (**a**) and DTG (**b**) curves of CNCs, SCNCs and their reinforced PBS composites at 7% loading; TGA curves of PBS/CNC (**c**) and PBS/SCNC (**d**) composites with increasing nanofiller content

delays the escape of volatile degradation products of PBS. Similar thermal degradation behavior was also demonstrated for PBS/CF composites (Liang et al. 2015). Thus, the stability of PBS/SCNC composites have been remarkably improved compared to that of PBS/CNC composites.

Mechanical properties

Figure 9 shows the effects of CNC or SCNC content on the mechanical properties of the PBS/CNC and PBS/SCNC nanocomposites including Young's modulus, yield strength, and elongation at break (%). As it is well known, PBS is a semi-crystalline polyester and show an obvious yielding and stable necking. Many studies illustrate that yield strength is a very important index to measure the mechanical properties of PBS in terms of practical properties (Aontee and Sutapun 2013; Li et al. 2017; Zeng et al. 2016). Both yield strength and Young's modulus increase continuously with increasing CNC (SCNC) content. When CNC (SCNC) content exceeds 3 wt%, yield strength gradually decreased, Young's modulus of nanocomposites keeps increasing. Comparing with PBS/CNC composites, PBS/SCNC composites show higher Young's modulus and yield strength. This should be contributed by homogenous dispersion of SCNCs in PBS/SCNC comparing to self-aggregation of CNCs in PBS matrix. In addition, more hydrogen bonds between PBS carbonyl groups and ester groups on main chains of SCNCs may improve interfacial compatibility between nanofillers and matrix. However, the introduction of superfluous nanofillers (such as 5 wt% and 7 wt% concentration) may cause the self-aggregation of CNCs and SCNCs and possible microphase separation in the composites. Above this, increased self-

Table 2 TGA data of CNCs, SCNCs and PBS based nanocomposites

Sample	$*T_{d(99\%)}$	$*T_{d(97\%)}$	$*T_{d(95\%)}$	$*T_{max}$ (°C)
CNCs	221	232	242	295
SCNCs	217	231	249	348
PBS	323	344	353	414
PBS/CNC (99/1)	343	358	366	412
PBS/CNC (97/3)	303	357	366	412
PBS/CNC (95/5)	275	333	359	412
PBS/CNC (93/7)	268	300	341	413
PBS/SCNC(99/1)	343	360	366	409
PBS/SCNC(97/3)	335	359	368	413
PBS/SCNC(95/5)	317	351	365	413
PBS/SCNC(93/7)	307	344	358	411

$*T_{d(99\%)}$ is temperature evaluated at 1 wt% weight loss. $T_{d(97\%)}$ is temperature evaluated at 3 wt% weight loss. $T_{d(95\%)}$ is temperature evaluated at 5 wt% weight loss. T_{max} is the temperature at maximum degradation rate

agglomeration of CNCs could then result in a sharp decline in mechanical properties of composites, which can be associated with FE-SEM images. Similar results are also reported by other researchers (Hu et al. 2015). Elongation at break of both PBS/CNC and PBS/SCNC nanocomposites show decreasing trend with increasing CNC (SCNC) content, the brittle fraction can be triggered by CNC (SCNC) aggregation at high contents.

Conclusion

In this work, cellulose nanocrystals (CNCs) was extracted from microcrystalline cellulose. After that, CNCs were modified by different mount of SAA to give succinic CNCs (SCNCs). The obtained SCNCs

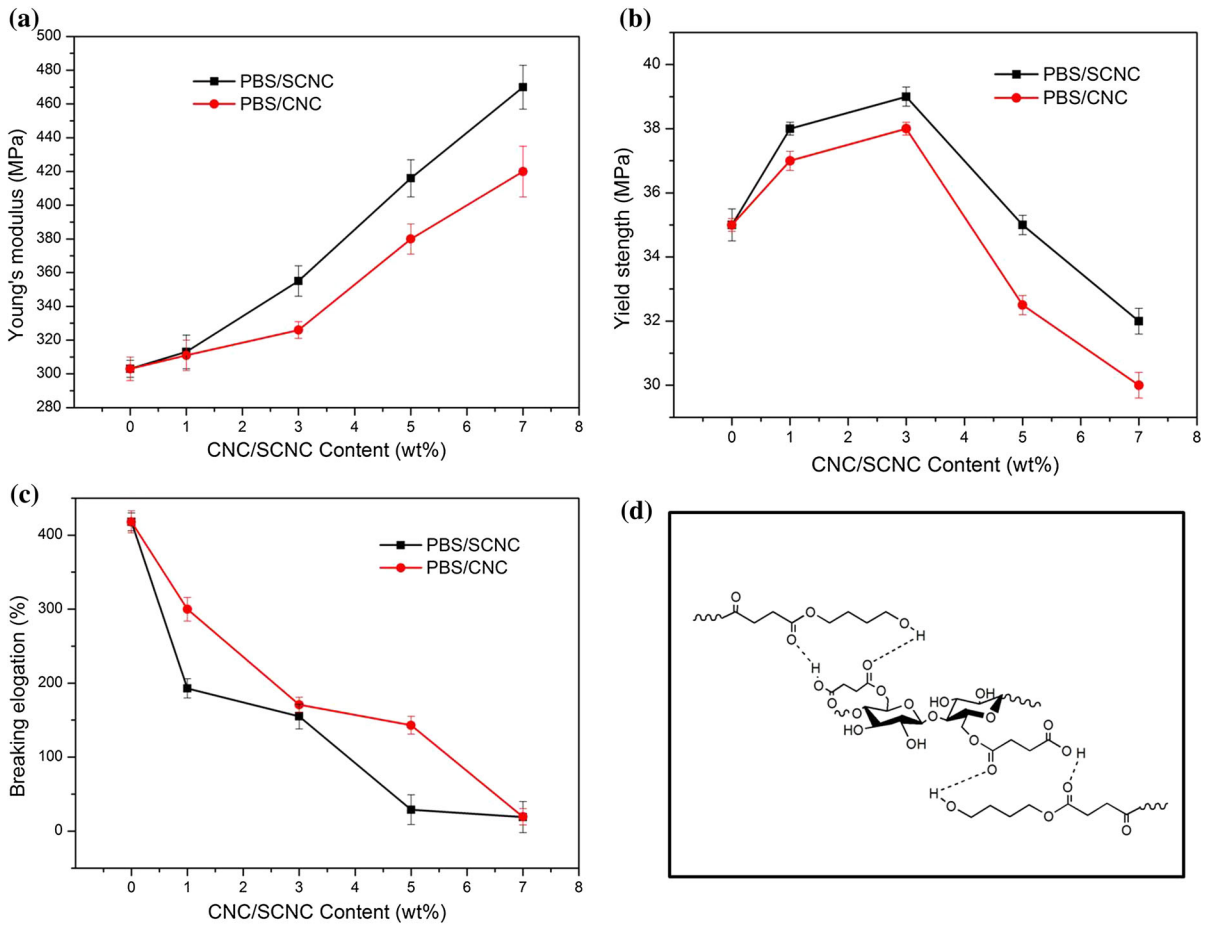

Fig. 9 Mechanical properties of nanocomposites: **a** Young's modulus, **b** yield strength, **c** elongation at break for nanocomposites with different CNC and SCNC content, **d** possible hydrogen bond effect between PBS chains and SCNC nanoparticles

and CNCs were then melt blended with PBS to give PBS-based nanocomposites.

(1) Morphological structure of CNCs is preserved after modification, which can be observed on field emission scanning electron microscopy (FE-SEM) images. Successful chemical structure modification of CNCs was verified by fourier transforms infrared spectroscopy (FTIR) and ^{13}C CP-MAS NMR test. Furthermore, SCNCs show strong hydrophobicity, and its hydrophobicity enhances with increasing amount of SAA confirmed by water contact angle measurement and dispersity test.
(2) Cryo-fractured surface of PBS-based nanocomposites reveals that small amount of CNCs can well-distributed in PBS matrix, when the CNC (SCNC) content exceeds 3 wt%, CNCs show more heavier self-aggregation and even phase separation compared with SCNCs dispersing in PBS matrix.
(3) Thermal stability of PBS are observably improved after the addition of SCNCs mainly due to less sulfate groups on SCNC surfaces than CNC surfaces, which can be measured by Zeta potential test and elemental analysis. Meanwhile, Young's modulus and yield strength of PBS/SCNC are higher than that of PBS/CNC nanocomposites, which is primarily attributed to the homogeneous dispersion of SCNC in PBS matrix, confirmed by FE-SEM images.

Acknowledgments The authors gratefully acknowledge Open Foundation of Key Laboratory of Advanced Textile Materials and Manufacturing Technology (Zhejiang Sci-Tech University), Education Ministry of China (No. 2017001) and Zhejiang Provincial Natural Science Foundation of China (No. LQ18E030010).

References

Angellier H, Molinaboisseau S, Dufresne A (2005) Mechanical properties of waxy maize starch nanocrystal reinforced natural rubber. Macromolecules 28(38):9161–9170

Aontee A, Sutapun W (2013) Effect of blend ratio on phase morphology and mechanical properties of high density polyethylene and poly (butylene succinate) blend. In: The international conference on multi-functional materials and structures, pp 555–559

Avolio R, Graziano V, Pereira YDF, Cocca M, Gentile G, Errico ME, Ambrogi V, Avella M (2015) Effect of cellulose structure and morphology on the properties of poly(-butylene succinate-*co*-butylene adipate) biocomposites. Carbohydr Polym 133:408–420

Bendahou A, Hajlane A, Dufresne A, Boufi S, Kaddami H (2014) Esterification and amidation for grafting long aliphatic chains on to cellulose nanocrystals: a comparative study. Res Chem Intermed 41:4293–4310

Braun B, Dorgan JR, Hollingsworth LO (2012) Supra-molecular ecobionanocomposites based on polylactide and cellulosic nanowhiskers: synthesis and properties. Biomacromolecules 13(7):2013–2019

Chen S, Cheng L, Huang H, Zou F, Zhao HP (2017) Fabrication and properties of poly(butylene succinate) biocomposites reinforced by waste silkworm silk fabric. Compos A Appl Sci Manuf 95:125–131

Content M (1997) Standard test methods of testing cellulose acetate propionate and cellulose acetate. ASTM, West Conshohocken

Coseri S, Biliuta G, Simionescu BC, Stana-Kleinschek K, Ribitsch V, Harabagiu V (2013) Oxidized cellulose—survey of the most recent achievements. Carbohydr Polym 93(1):207–215

Espino-Pérez E, Bras J, Ducruet V, Guinault A, Dufresne A, Domenek S (2013) Influence of chemical surface modification of cellulose nanowhiskers on thermal, mechanical, and barrier properties of poly(lactide) based bionanocomposites. Eur Polym J 49(10):3144–3154

Flores ED, Funabashi M, Kunioka M (2009) Mechanical properties and biomass carbon ratios of poly(butylene succinate) composites filled with starch and cellulose filler using furfural as plasticizer. J Appl Polym Sci 112(6):3410–3417

Fortunati E, Armentano I, Iannoni A, Kenny JM (2010) Development and thermal behaviour of ternary PLA matrix composites. Polym Degrad Stab 95(11):2200–2206

Fortunati E, Peltzer M, Armentano I, Torre L, Jiménez A, Kenny JM (2012) Effects of modified cellulose nanocrystals on the barrier and migration properties of PLA nano-biocomposites. Carbohydr Polym 90(2):948–956

Fujisawa S, Okita Y, Saito T, Togawa E, Isogai A (2011) Formation of *N*-acylureas on the surface of TEMPO-oxidized cellulose nanofibril with carbodiimide in DMF. Cellulose 18(5):1191–1199

Glova AD, Falkovich SG, Larin SV, Mezhenskaia DA, Lukasheva NV, Nazarychev VM, Tolmachev DA, Mercurieva AA, Kenny JM, Lyulin SV (2016) Poly(lactic acid)-based nanocomposites filled with cellulose nanocrystals with modified surface: all-atom molecular dynamics simulations. Polym Int 65(8):892–898

Hamad WY, Hu TQ (2010) Structure–process–yield interrelations in nanocrystalline cellulose extraction. Can J Chem Eng 88(3):392–402

Hashaikeh R, Krishnamachari P, Samad Y (2015) Nanomanifestations of cellulose: applications for biodegradable composites. Springer, Berlin

Hu F, Lin N, Chang PR, Huang J (2015) Reinforcement and nucleation of acetylated cellulose nanocrystals in foamed polyester composites. Carbohydr Polym 129:208–215

Jiang F, Esker AR, Roman M (2010) Acid-catalyzed and solvolytic desulfation of H_2SO_4-hydrolyzed cellulose

nanocrystals. Langmuir ACS J Surf Colloids 26(23):17919–17925
Jiménez A, Ruseckaite RA (2007) Binary mixtures based on polycaprolactone and cellulose derivatives. J Therm Anal Calorim 88(3):851–856
Li Y, Fu Q, Ming W, Zeng J (2017) Morphology, crystallization and rheological behavior in poly(butylene succinate)/cellulose nanocrystal nanocomposites fabricated by solution coagulation. Carbohydr Polym 164:75
Liang Z, Pan P, Zhu B, Dong T, Inoue Y (2010) Mechanical and thermal properties of poly(butylene succinate)/plant fiber biodegradable composite. J Appl Polym Sci 115(6):3559–3567
Liang J, Ding C, Wei Z, Sang L, Song P, Chen G, Chang Y, Xu J, Zhang W (2015) Mechanical, morphology, and thermal properties of carbon fiber reinforced poly(butylene succinate) composites. Polym Compos 36(7):1335–1345
Likittheerakarn S, Kurdpradid S, Smittipornpun N, Sritapunya T (2017) Comparison of mechanical properties of biocomposites between polybutylene succinate/corn silk and polybutylene succinate/cellulose extracted from corn silk. Key Eng Mater 737:275–280
Lin N, Dufresne A (2014) Surface chemistry, morphological analysis and properties of cellulose nanocrystals with gradiented sulfation degrees. Nanoscale 6(10):5384–5393
Lin N, Huang J, Chang PR, Feng J, Yu J (2011) Surface acetylation of cellulose nanocrystal and its reinforcing function in poly(lactic acid). Carbohydr Polym 83(4):1834–1842
Luzi F, Fortunati E, Jiménez A, Puglia D, Pezzolla D, Gigliotti G, Kenny JM, Chiralt A, Torre L (2016) Production and characterization of PLA_PBS biodegradable blends reinforced with cellulose nanocrystals extracted from hemp fibres. Ind Crops Prod 93:276–289
Miao C, Hamad WY (2016) Alkenylation of cellulose nanocrystals (CNC) and their applications. Polymer 101:338–346
Miyata T, Masuko T (1998) Crystallization behaviour of poly(tetramethylene succinate). Polymer 39(6–7):1399–1404
Motte HDL, Hasani M, Brelid H, Westman G (2011) Molecular characterization of hydrolyzed cationized nanocrystalline cellulose, cotton cellulose and softwood kraft pulp using high resolution 1D and 2D NMR. Carbohydr Polym 85(4):738–746
Nagalakshmaiah M, El Kissi N, Dufresne A (2016) Ionic compatibilization of cellulose nanocrystals with quaternary ammonium salt and their melt extrusion with polypropylene. ACS Appl Mater Interfaces 8(13):8755–8764
Nampoothiri KM, Nair NR, John RP (2010) An overview of the recent developments in polylactide (PLA) research. Bioresour Technol 101(22):8493–8501
Ng HM, Sin LT, Tee TT, Bee ST, Hui D, Low CY, Rahmat AR (2015) Extraction of cellulose nanocrystals from plant sources for application as reinforcing agent in polymers. Compos B Eng 75:176–200
Ogawa K, Hirai I, Shimasaki C, Yoshimura T, Ono S, Rengakuji S, Nakamura Y, Yamazaki I (1999) Simple determination method of degree of substitution for starch acetate. Bull Chem Soc Jpn 72(12):2785–2790
Papageorgiou GZ, Bikiaris DN (2005) Crystallization and melting behavior of three biodegradable poly(alkylene succinates). A comparative study. Polymer 46(26):12081–12092
Paralikar SA, Simonsen J, Lombardi J (2008) Poly(vinyl alcohol)/cellulose nanocrystal barrier membranes. J Membr Sci 320(1):248–258
Pinheiro IF, Ferreira FV, Souza DHS, Gouveia RF, Lona LMF, Morales AR, Mei LHI (2017) Mechanical, rheological and degradation properties of PBAT nanocomposites reinforced by functionalized cellulose nanocrystals. Eur Polym J 97:356–365
Poaty B, Vardanyan V, Wilczak L, Chauve G, Riedl B (2014) Modification of cellulose nanocrystals as reinforcement derivatives for wood coatings. Prog Org Coat 77(4):813–820
Ragauskas AJ, Williams CK, Davison BH, Britovsek G, Cairney J, Eckert CA, Frederick WJ Jr., Hallett JP, Leak DJ, Liotta CL (2006) The path forward for biofuels and biomaterials. Science 311(5760):484–489
Shang W, Huang J, Luo H, Chang PR, Feng J, Xie G (2013) Hydrophobic modification of cellulose nanocrystal via covalently grafting of castor oil. Cellulose 20(1):179–190
Silverio HA, Neto WPF, Dantas ON, Pasquini D (2013) Extraction and characterization of cellulose nanocrystals from corncob for application as reinforcing agent in nanocomposites. Ind Crops Prod 44(2):427–436
Spinella S, Re GL, Liu B, Dorgan J, Habibi Y, Leclère P, Raquez JM, Dubois P, Gross RA (2015) Polylactide/cellulose nanocrystal nanocomposites: efficient routes for nanofiber modification and effects of nanofiber chemistry on PLA reinforcement. Polymer 65:9–17
Tang Y, Yang S, Zhang N, Zhang J (2014) Preparation and characterization of nanocrystalline cellulose via low-intensity ultrasonic-assisted sulfuric acid hydrolysis. Cellulose 21(1):335–346
Vahik K, Pochan D (2004) Unusual crystallization behavior of organoclay reinforced poly(L-lactic acid) nanocomposites. Macromolecules 37(17):6480–6491
Xue MD, Revol JF, Gray DG (1998) Effect of microcrystallite preparation conditions on the formation of colloid crystals of cellulose. Cellulose 5(1):19–32
Zeng RT, Hu W, Wang M, Zhang SD, Zeng JB (2016) Morphology, rheological and crystallization behavior in non-covalently functionalized carbon nanotube reinforced poly(butylene succinate) nanocomposites with low percolation threshold. Polym Test 50:182–190
Zhang X, Yong Z (2016) Reinforcement effect of poly(butylene succinate) (PBS)-grafted cellulose nanocrystal on toughened PBS/polylactic acid blends. Carbohydr Polym 140:374–382
Zhou M, Li Y, He C, Jin T, Wang K, Fu Q (2014) Interfacial crystallization enhanced interfacial interaction of poly(-butylene succinate)/ramie fiber biocomposites using dopamine as a modifier. Compos Sci Technol 91(2):22–29
Zhou L, He H, Li MC, Huang S, Mei C, Wu Q (2018a) Enhancing mechanical properties of poly(lactic acid) through its in situ crosslinking with maleic anhydride-modified cellulose nanocrystals from cottonseed hulls. Ind Crops Prod 112:449–459

Zhou L, He H, Li MC, Huang S, Mei C, Wu Q (2018b) Grafting polycaprolactone diol onto cellulose nanocrystals via click chemistry: enhancing thermal stability and hydrophobic property. Carbohydr Polym 189:331–341

Zhu B, Li J, He Y, Osanai Y, Matsumura S, Inoue Y (2003) Thermal and infrared spectroscopic studies on hydrogen-bonding interaction of biodegradable poly(3-hydroxybutyrate)s with natural polyphenol catechin. Green Chem 5(5):580–586